NANO LETTERS

2009
Vol. 9, No. 1
479-484

Control of Shape and Material Composition of Solid-State Nanopores

Meng-Yue Wu,[†] Ralph M. M. Smeets,[†] Mathijs Zandbergen,[‡] Ulrike Ziese,[†] Diego Krapf,[†,§] Philip E. Batson,[‡] Nynke H. Dekker,[†] Cees Dekker,[†] and Henny W. Zandbergen*[,†]

Kavli Institute of Nanoscience, Delft University of Technology, Lorentzweg 1, 2628 CJ Delft, The Netherlands, and IBM Thomas J. Watson Research Center, Yorktown Heights, New York 10598

Received November 28, 2008

ABSTRACT

Solid-state nanopores fabricated by a high-intensity electron beam in ceramic membranes can be fine-tuned on three-dimensional geometry and composition by choice of materials and beam sculpting conditions. For similar beam conditions, 8 nm diameter nanopores fabricated in membranes containing SiO_2 show large depletion areas (70 nm in radius) with small sidewall angles (55°), whereas those made in SiN membranes show small depletion areas (40 nm) with larger sidewall angles (75°). Three-dimensional electron tomograms of nanopores fabricated in a SiO_2/SiN/SiO_2 membrane show a biconical shape with symmetric top and bottom and indicate a mixing of SiN and SiO_2 layers up to 30 nm from the edge of nanopore, with Si-rich particles throughout the membrane. Electron-energy-loss spectroscopy (EELS) reveals that the oxygen/nitrogen ratio near the pore depends on the beam sculpting conditions.

Solid-state nanopores are used to detect and characterize DNA and RNA with single-molecule resolution,[1] comparable to the translocation measurements performed on biological phospholipid-embedded protein channels.[2] They have significant advantages over protein channels as they are functional in a wider range of temperatures, solvents, and voltages and offer possibilities for device integration and tunability in the pore dimensions. A nanopore can be readily formed in thin membranes by an electron beam in a TEM.[3−5] This TEM-based method provides an advantage of excellent size control as the nanopore can directly be visualized during drilling process. In addition, the shape of the nanopore can be controlled, provided that the electron beam is very well aligned and the specimen drift is low. The sidewall abruptness, which is an important factor in the analysis of DNA translocation through nanopores, can be tuned with the drilling conditions (beam size, beam intensity) and on the sample composition. Notably, a very different sidewall abruptness was observed in nanopores fabricated in 40 nm SiO_2/SiN[4] and 50 nm Si_3N_4 membranes,[5,6] demanding further investigation. Another very important factor in the analysis of DNA translocation is the surface composition of the nanopore, as Smeets et al. [7] have suggested following examination of a range of nanopores. Since SiN and SiO_2 may yield different surface compositions resulting in different hydrophilicities, the control of surface charge via TEM-engineered material properties is an interesting perspective.

To better control the shape and material composition of solid-state nanopores, we here use electron-energy-loss spectroscopy (EELS), energy-filtered TEM (EFTEM), electron tomography, scanning transmission-electron microscopy (STEM), and high-resolution transmission-electron microscopy (HRTEM) to measure the shape and composition of the nanopore as a function of electron-beam drilling procedures and membrane composition. Electron tomography shows that the shape of the pore is mirror symmetric about the middle plane of the membrane and yields a thickness variation in good agreement with EFTEM data. By combining EELS and HRTEM, we obtain information on the material surrounding the pore; we show that small Si-rich particles are formed by a high-intensity electron beam in the membranes that contain SiO_2, but not in those formed in pure SiN. These small Si-rich particles are found throughout the membrane in the vicinity of the pore's rim, and indicate a thorough local mixing of nitride and oxide layers that is controlled by the electron beam. Furthermore, by combining EELS and STEM, we show that the oxygen and nitrogen composition in the region surrounding the nanopore is sensitive to the drilling conditions in the TEM.

Membranes were fabricated using standard semiconductor microfabrication processes. First, the following three-layer

* To whom correspondence should be addressed. E-mail: h.w.zandbergen@tnw.tudelft.nl. Fax: +31-15-2786730.
[†] Delft University of Technology.
[‡] IBM Thomas J. Watson Research Center.
[§] Present address: Electrical and Computer Engineering, Colorado State University, Fort Collins, Colorado 80523-1373.

10.1021/nl803613s CCC: $40.75
Published on Web 12/09/2008

structure was deposited on both sides of a 20−30 Ωcm, boron-doped, Si <100> wafer by low-pressure chemical vapor deposition (LPCVD): 20−60 nm of low-stress silicon-rich silicon nitride (SiN), followed by 200 nm of SiO_2, and a 500 nm thick capping layer of low stress SiN. Next, square windows were patterned in the backside layers using e-beam lithography and CHF_3 reactive ion etching. Using the backside SiN as a mask, the Si substrate was anisotropically etched in KOH solution (29 wt %) at 80 °C during 8 h. Free-standing 50 × 50 μm^2 membranes consisting of the three-layer stack were realized. In the middle of the membrane, a 5 μm wide region was thinned to expose only the lowermost 20−60 nm SiN layer. For this, the capping SiN and SiO_2 layers were removed by reactive ion etching and wet HF etching, respectively. The final fabrication step for the triple layer membrane involves the deposition of a 20 nm of silicon oxide film by sputtering in Ar plasma on both sides of the SiN membrane. A thin foil sample of amorphous SiO_2 was prepared using standard plan-view TEM sample preparation methods.

The nanopores were drilled and monitored using a field emission FEI Tecnai (S)TEM operated at an accelerating voltage of 200 kV. The (S)TEM system included a monochromator and a high-resolution Gatan Imaging Filter (HRGIF).[8,9] EELS spectra were obtained with the monochromator in off-mode since the intrinsic widths of the EELS peaks of Si, N, and O do not require the high resolution. Moreover, the higher brightness in off-mode allows a quicker formation of the nanopores. An electron beam with a diameter between 2 to 10 nm (full width at half-maximum height, fwhm) and a beam current of 2−7 nA was used for drilling. The N and O compositions were acquired with the microscope operant in STEM mode with a spot size about 0.5 nm, a camera length of 30−50 mm, a HRGIF entrance aperture of 2 mm, and an energy dispersion of either 0.5 or 0.2 eV/pixel. The energy-filtered transmission-electron microscopy (EFTEM) images were typically recorded using a 5 mm HRGIF entrance aperture and a 4 eV energy window (with the exception of a 10 eV energy window for the thickness map). Note that all experiments were repeated several times but only representative results are shown here.

TEM tomography using a Tecnai 20 was performed on a 20 nm nanopore in a SiO_2/SiN/SiO_2 membrane. This nanopore was enlarged by a ∼20 nm electron probe starting from an 8 nm nanopore that had previously been fabricated by a ∼10 nm electron probe with a beam current of 10−15 nA in a Philips 300UT microscope operated at 300 kV. Double-axis tilt series of 140 images for each axis were acquired from −70 to 70° with a tilt increment of 1°. IMOD software[10] was used to compute 3D reconstructions from the tilt series. A pixel size of 0.72 nm was obtained for the final reconstruction. The resulting three-dimensional structure of the nanopore was visualized using the surface reconstruction function included in Amira 4.1 (Mercury). To avoid electron-beam-induced changes during the tilt series, a low current density was used, and the total dose was ∼8 × 10^4 e/nm^2. No changes on the nanopore could be detected during the tilt series recording.

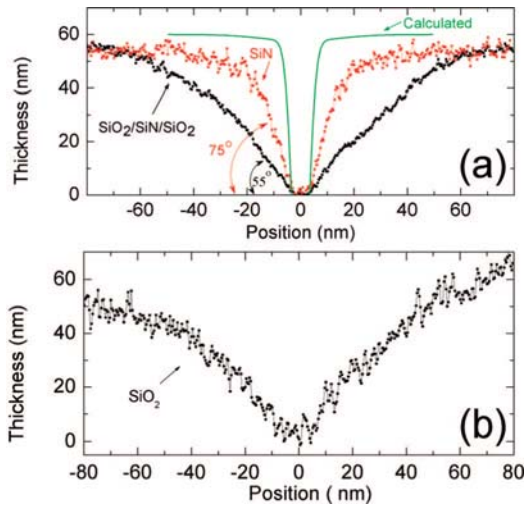

Figure 1. Measured and calculated thickness variation profiles. (a) Black, an 8 nm nanopore in 60 nm SiO_2/SiN/SiO_2 membrane; red, a 10 nm nanopore in ∼60 nm SiN membrane; green, a calculated 8 nm nanopore assuming a linear mass loss with respect to the electron beam intensity. Electron probes (9 and 45 nm) were used. The total dose of the 45 nm probe is 1/10 of the total dose of the 9 nm probe. (b) A 10 nm nanopore in an amorphous SiO_2 foil.

For the experiments involving drilling using a very small spot size, a STEM located at IBM in Yorktown Heights was used, which is based on a VG Microscopes HB501 STEM with the addition of a quadrupole−octupole aberration corrector.[11] The electron beam employed had a spot size of 0.1−0.15 nm and a current of 30−50 pA at 120 kV, and these experiments were performed on a 40 nm thick SiN membrane.

Nanopores can be fabricated in numerous types of membranes. Here we compare the thickness profiles of nanopores drilled in a single SiN membrane (20−60 nm in thickness), a triple layer SiO_2/SiN/SiO_2 membrane (20/20/20 nm) and also a pure SiO_2 foil. In Figure 1, we plot the thickness variations surrounding a 8 nm diameter nanopore in a 60 nm thick SiO_2/SiN/SiO_2 membrane, an ∼10 nm diameter nanopore in an ∼60 nm SiN membrane, and an ∼10 nm diameter nanopore in a pure amorphous SiO_2 membrane fabricated under similar drilling conditions (two beam sizes were used: a 9 nm (fwhm) beam for drilling and a 36−54 nm beam for short inspection of the nanopore (∼3% of drilling time)). A mean free path of 180 nm (calculated using the formulas in ref 12) was used to obtain the absolute thickness value of all three membranes. An uncertainty of ∼3% in the mean free path is expected as composition changes from pure Si to triple layer. The thickness profile in SiN membrane shows a sidewall angle of about 75° and a depletion area (<90% original thickness) of about 40 nm in radius, which is similar to the result reported by Kim et al.[5,6] In contrast, the edge of the nanopore in a SiO_2/SiN/SiO_2 membrane is more wedge-shaped with a sidewall angle about 55° and a depletion area of about 70 nm in radius, similar to that in a SiN/SiO_2 double layer membrane that we reported previously.[4] Nanopores formed in pure SiO_2 membranes were found to have a geometry that is comparable to that found in nanopores formed in the triple layer

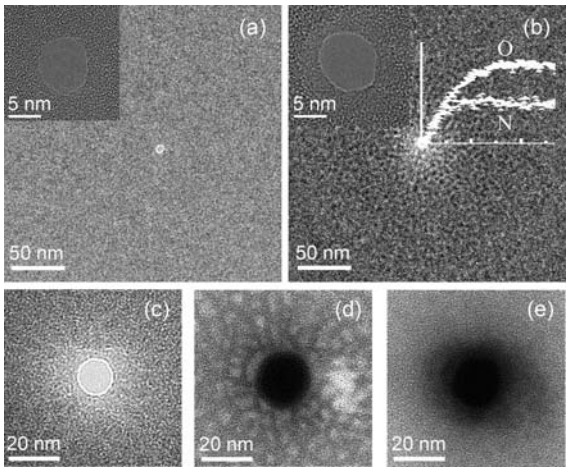

Figure 2. TEM images of two nanopores with sizes of 8 nm fabricated in (a) 20 nm SiN membrane and (b) 60 nm SiO_2/SiN/SiO_2 membrane under similar drilling conditions. The inset shows HRTEM images of these nanopores. The inset profile in (b) is the distribution of O and N. (c−e) EFTEM images of a 14 nm nanopore in a SiO_2/SiN/SiO_2 membrane acquired with different energy windows (c) −2−2 eV, (d) 15−19 eV and (e) 21−25 eV.

(Figure 1b). In all three cases, the large extent of the depletion area compared to the size of the electron beam is remarkable. Assuming a Gaussian beam profile and a material loss that is linear with beam dose, the material depletion profile for the experimental conditions we used is calculated (Figure 1, green line). Comparing this estimated depletion profile with the experimental shapes (Figure 1, red and black dotted lines), we conclude that there must be a lateral displacement of material. Similar phenomena were also observed when a very small beam (0.1−0.15 nm) was used to drill nanopores in 40 nm thick SiN membrane whereby the membrane was thinned in an area with a radius of 4 nm (data not shown).

In addition to the difference in the shape of the nanopores fabricated in SiN membranes versus SiO_2/SiN/SiO_2 or pure SiO_2 membranes, we also observed an effect of membrane composition on the formation of small Si-rich particles in the membranes. Figure 2a,b shows images of two 8 nm diameter nanopores fabricated in a 20 nm SiN and in a 60 nm SiO_2/SiN/SiO_2 membranes under similar drilling conditions, respectively. Small particles with a size of about 3 nm can be clearly seen in all the membranes that contain a SiO_2 layer (Figure 2b), but not in the SiN single layer membranes (Figure 2a). To exclude an effect of the film thickness, we also confirmed that 40 and 60 nm SiN membranes did not show the formation of particles. These small particles were identified as Si-rich particles by EFTEM using a 15−19 eV energy window, which included the bulk plasmon peak of Si at 16.7 eV, while excluding the plasmon peaks of SiN and SiO_2 near 22.8 eV. Figure 1c−e shows EFTEM images of a 14 nm nanopore in SiO_2/SiN/SiO_2 membrane with different energy windows: an elastic image (−2 to +2 eV; Figure 1c), an EFTEM image around the Si bulk plasmon (Figure 2d), and an EFTEM image around the bulk plasmon for SiN and SiO_2 (Figure 2e). The small particles are clearly visible in the 15−19 eV EFTEM image (Figure 2d), showing that these particles are Si-rich. No lattice fringes were found in HREM images of these particles. More detailed information of valence states of Si in the particles cannot be given due to their intrinsic energy widths. Dori et al.[13] have reported that in substoichiometric oxides excess silicon is present either as nanometer-sized silicon islands or as submicroscopic silicon oxides of varying stoichiometry. However, the possibility that the electron beam might modify the valence state of Si was not discussed by Dori et al. Chen et al.[14] found that amorphous Si dots, or wires surrounded by SiO_{2-x}, can be formed in amorphous 15 nm thick SiO_2 films by a high-intensity 100 keV focused electron probe.

To determine the membrane composition at which the small Si-rich particles start to form, a line scan was performed across the nanopore (see the inset profile in Figure 2b). Around the nanopores in SiO_2/SiN/SiO_2 membranes, the average radius of the O depletion area is about 75 nm, whereas that of the N depletion area is about 30 nm. Comparing the locations of the small Si-rich particles in the TEM image with the oxygen composition distribution at the rim of the nanopore, it can be seen that the particles are present in the area where ∼20% oxygen is lost. Interestingly, the area of nitrogen loss in the case of a sandwich between two SiO_2 layers is larger (by about 10 nm) than the loss area of a single SiN layer, which holds for both 20 and 60 nm thick SiN films. This indicates that SiN reacts with the SiO_2 layers in that area of the triple layer.

Using our control of the electron beam, we can fine-tune the size of the nanopore. In a previous paper, we have already reported that the nanopore size can be reduced, but here we demonstrate that enlargement is also possible via this technique.[15] Two methods were used for pore enlargement: (1) we defocused the small beam so that the rim of the nanopore is equally irradiated, and (2) we continue the drilling with the tail of the focused beam. Figure 3 plots the thickness profiles of two nanopores that are enlarged from 8 to 18 nm in SiO_2/SiN/SiO_2 triple layer membranes. The profiles shown in Figure 3a are from the same pore before and after enlargement with method (1) using a ∼20 nm defocused electron beam, whereas the profiles in Figure 3c are from the initial small pore and its enlargement through method (2) using a focused ∼10 nm electron beam. Both enlargements result in changes in the nanopore geometry. However, the changes are different, as can be seen from the difference profiles of the thicknesses before and after nanopore enlargements by these two methods (Figure 3b,d). When method (2) is employed, the maximum loss of material occurs at ∼10 nm from the edge whereas material is lost in a region up to ∼ 20 nm from the edge of nanopore. This results in a steeper sidewall, for example, the nanopore becomes more tunnel-like. In contrast, when method (1) is employed, the maximum loss of matter occurs at ∼20 nm from the edge and the overall material loss range is in a ∼45 nm region from the edge of the nanopore. Consequently, with a defocused beam the surrounding of the nanopore becomes thinner while keeping the sidewall angle nearly unchanged.

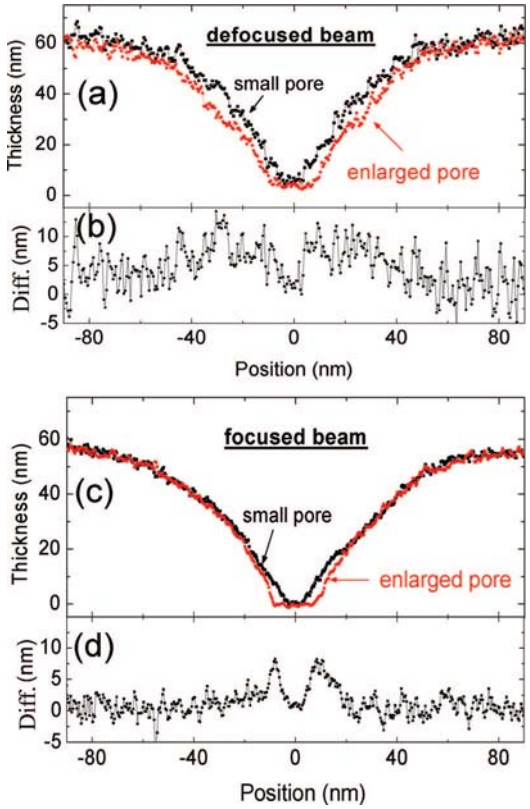

Figure 3. Thickness variation profiles (acquired by EFTEM) around nanopores before and after enlargement and the respective difference profiles via the use of (a) an ~20 nm defocused beam and (c) an ~10 nm focused beam.

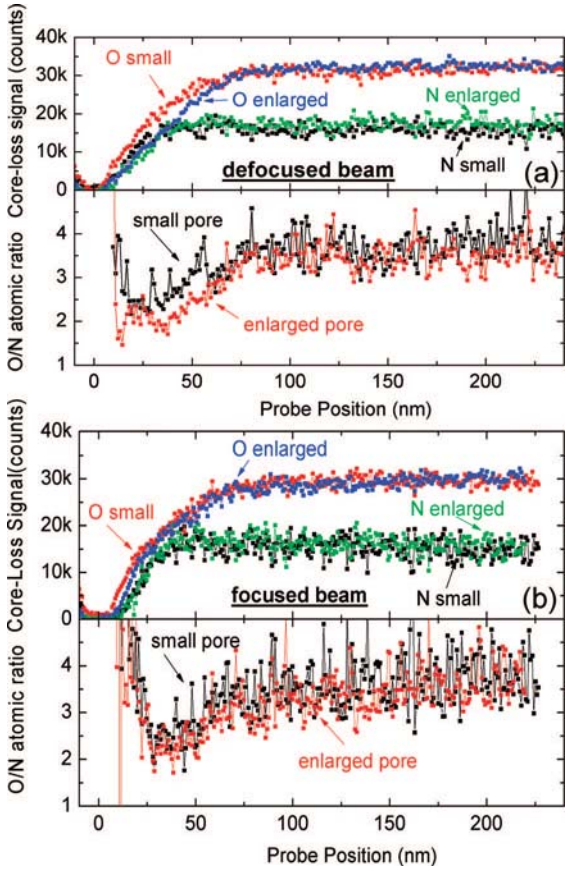

Figure 4. The distribution of N and O atoms before and after enlargement by the electron beam in two different ways. (a) Defocused beam and (b) highly focused beam. An O/N cross section ratio of 1.87 was used in O/N atomic ratio profile as appropriate for our experiment condition. The data of all O/N profiles are plotted starting at the edge of the large nanopore.

The two different ways to enlarge a small nanopore in a ~60 nm SiO_2/SiN/SiO_2 membrane also lead to different O/N ratios near the edge of the nanopore, as can be seen in Figure 4. In Figure 4a,b, we compare the O and N composition before and after enlargement for the two enlargement techniques. Using the defocused beam, the O/N ratio is smaller in the depletion area than before enlargement (see Figure 4a). Through the use of the highly focused beam, the O/N ratio does not change significantly (see Figure 4b). Note that the O and N spectra were acquired simultaneously under low beam intensity conditions to avoid additional material alteration by the electron probe. This results in higher scatter in the N signal since the O/N atomic ratio is about 3.5 in the initial sample. Consequently the O/N profiles are somewhat noisy, but the signal-to-noise is sufficient to allow us to reproducibly observe the trends of the changes in O/N by the two different enlargement methods.

Finally, to determine the 3D geometry of the nanopore, TEM tomography was carried out on a ~20 nm nanopore fabricated in a ~60 nm SiO_2/SiN/SiO_2 membrane. The resulting three-dimensional shape is shown in Figure 5a. Note that the shape of the pore is mirror symmetric, with the mirror plane in the middle of the trilayer. Although this 20 nm nanopore was fabricated with different beam settings in the primary beam energy and beam current, the thickness variation is similar to that of the ~20 nm nanopore fabricated in a ~60 nm SiO_2/SiN/SiO_2 membrane shown in Figure 3a. A comparison of the two thickness profiles is given in Figure 5b. The sidewall angle β indicated in the inset of Figure 5b can be simply calculated from the sidewall angle α measured from the thickness profile as $\beta = 2\ \arctan(\tan(\alpha)/2)$.

In addition to the three-dimensional shape of nanopore, we obtained the distribution of Si-rich particles from TEM tomography. Several slices of the tomogram are depicted in Figure 5c−h. In the first 30 nm from the edge of the pore, the Si-rich particles are present throughout the entire thickness of the film. In the area between 30 and 70 nm from the edge, the Si rich particles decrease gradually in number density in SiO_2 layer, and they are not present in the middle SiN layer. This last observation, in combination with the fact that there is no significant loss in N in this area, indicates that in this area there is no change in the SiN layer both is shape and in composition, and thus that no mixing with the SiO_2 layers occurred.

The tomography allows us to distinguish two areas surrounding the nanopore (see Figure 5): Area 1 with a radius of about 30 nm, including the pore and its direct surroundings, and Area 2 in a region with a radius between 30 and 70 nm radii, where there is significant O loss and no N loss. We assume that in Area 1, which is the area irradiated with a high intensity electron beam, the material almost behaves as a liquid during the drilling. This assumption is supported

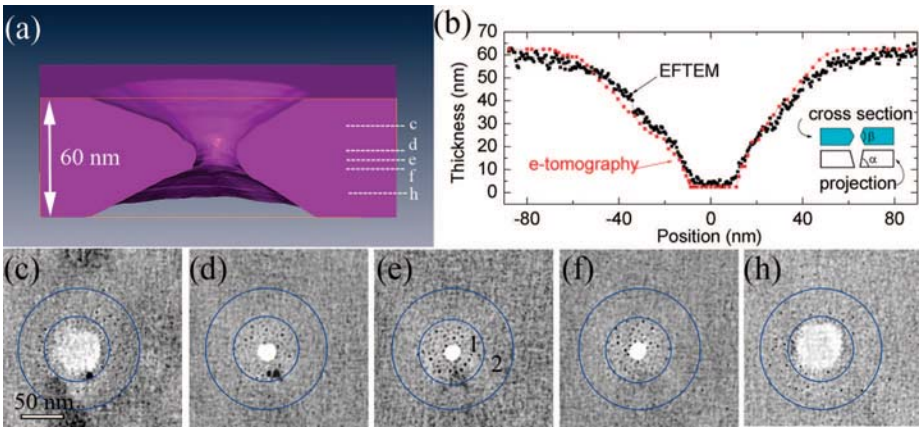

Figure 5. Three-dimensional structure of a 20 nm nanopore fabricated in $SiO_2/SiN/SiO_2$ membrane. (a) Surface reconstruction image. (b) Comparison of the thickness profiles deduced from the three-dimensional reconstruction and the one of the 18 nm nanopore shown in Figure 3a. (c−h) Five slices through the membrane with cutting positions indicated in panel a. The blue circles in panels c−h have 30 and 70 nm radii delineating the two different areas discussed in the text.

by the constant changes in contrast observed (movie, Supporting Information), which indicates very rapid changes in the atoms' positions. This is quite plausible as 200 keV electrons can easily break O and N bonds. It is also supported by experiments by Kimoto et al.[16] on $SiO_2/Si_3N_4/SiO_xN_y/Si$ multilayers, which showed for instance that O atoms can be dragged by the electron beam from the SiO_2 layer into the Si_3N_4 layer. Such liquidlike behavior would lead to mixing of O and N over the liquidlike volume, and concomitantly Si rich particles all throughout the membrane thickness, as we observed. If the beam is displaced or enlarged, new volume is added to the liquidlike part, and if the added volume has a different composition, the overall composition of the liquidlike volume will change. This explains why more N-rich material is found near the edge of the pore when an enlarged beam is used. This effect allows us to change the composition of the rim. Another effect of the liquidlike behavior is that during the removal of material, the surfaces on the top and bottom of the membrane are governed by a minimization of the surface energy, and thus that top and bottom parts of the pore will have very similar shapes and will be mirror symmetric in Area 1. This is in contrast with crystalline materials where the formation of the pore by a high electron beam starts with the formation of voids and a hole in the bottom side of the specimen and where the top side at first shows almost no changes.[17,18] Our results imply that one could in principle deposit a layer on the membrane after the pore formation and mix this into the membrane material with the electron beam, thereby fine-tuning the chemical composition. In Area 2, diffusion along the membrane normal does not occur because the negligible nitrogen loss in Area 2 indicates that the SiN layer remains intact in this region. Thus, lateral diffusion should take place. From the mirror symmetry in Area 2, we conclude that sputtering is not a dominant mechanism, which is consistent with the low exposure to the electron beam.

Our results suggest that the shape of the edge of the nanopore can be optimized by the choice of the composition of the membrane in particular using multiphase membranes, like the $SiO_2/SiN/SiO_2$ membranes used here. Since the local surface roughness and hydrophobicity are speculated to be the reason for nanobubble formation, a prominent source of noise in solid-state nanopores,[16] it is advantageous to be able to engineer the composition near the nanopore. Control over the three-dimensional structure and local properties of nanopores is of importance to improve the reliability of these sensors,[19,20] and to interpret results of translocation measurements.[7]

In summary, solid-state nanopores can be fabricated in membranes with a range of SiN/SiO_2 compositions by a high-intensity electron beam. The final geometry of the nanopore is dependent on material composition and drilling conditions. In addition, once a nanopore is created, the local composition at the edge can be changed by mixing in material of the membrane part that has a composition different from the edge, which is possible due to the fluidlike behavior of the area that is irradiated with an intense electron beam. The results given in this paper enable the fabrication of improved and well-characterized nanopores.

Acknowledgment. This work was financially supported by the Dutch foundation for Fundamental Research on Matter (FOM) and The Netherlands Organization for Scientific Research (NWO). N.H.D. acknowledges funding from the European Young Investigators program (EURYI) of the European Science Foundation (ESF). The authors would like to thank Anna Carlsson of the FEI Company for image acquisition for 3D tomography and Gregory Pandraud of the Delft Institute of Microelectronics and Submicron Technology, Delft University of Technology for a supply of SiN samples.

Supporting Information Available: High resolution electron microscopy movie of the formation of a nanopore in a 60 nm $SiO_2/SiN/SiO_2$ membrane. An ~10 nm electron probe with primary energy of 300 keV and beam current of 7 nA is used for drilling. Because of the dynamical range of the CCD, there is no contrast in the area with very high intensity. An enlarged beam has to be used to view the changes induced by the focused beam in the material. The

material under the focused beam becomes thinner and thinner. Once we see clearly a 5 nm nanopore is created, we defocus the beam. The nanopore increases in size until the electron beam is indeed defocused sufficiently. The nanopore shrinks continually to 5 nm as we refocus the beam (∼100 nm). This material is available free of charge via the Internet at http://pubs.acs.org.

References

(1) Dekker, C. *Nat. Nanotech.* **2007**, *2*, 209.
(2) Kasianowicz, J. J.; Brandin, E.; Branton, D.; Demer, D. W. *Proc. Nat. Acad. Sci. U.S.A.* **1996**, *93*, 13770.
(3) Storm, A. J.; Chen, J. H.; Ling, X. S.; Zandbergen, H. W.; Dekker, C. *Nat. Mater.* **2003**, *2*, 537.
(4) Wu, M.-Y.; Krapf, D.; Zandbergen, M.; Zandbergen, H. W.; Batson, P. E. *Applied Phys. Lett.* **2005**, *87*, 113106.
(5) Kim, M. J.; Wanunu, M.; Bell, D. C.; Meller, A. *Adv. Mater.* **2006**, *18*, 3149.
(6) Kim, M. J.; McNally, B.; Murata, K.; Meller, A. *Nanotechnology* **2007**, *18*, 205302.
(7) Smeets, R. M. M.; Keyser, U. F.; Krapf, D.; Wu, M.-Y.; Dekker, N. H.; Dekker, C. *Nano Lett.* **2006**, *6*, 89.
(8) Tiemeijer, P. C.; van Lin, J; H, A.; de Jong, A. F. *Microsc. Microanal.* **2001**, *7* (suppl. 2), 1130–1131.
(9) Lazar, S.; Botton, G. A.; Wu, M.-Y.; Tichelaar, F. D.; Zandbergen, H. W. *Ultramicroscopy* **2003**, *96*, 535.
(10) Kremer, J. R.; Mastronarde, D. N.; McIntosh, J. R. *J. Struct. Biol.* **1996**, *116*, 71.
(11) Batson, P. E.; Dellby, N.; Krivanek, O. L. *Nature* **2002**, *418*, 8.
(12) Egerton, R. F. Plenum Press: New York, 1996; Vol. 305.
(13) Dori, L.; Bruley, J.; DiMaria, D. J.; Batson, P. E.; Tornello, J.; Arienzo, M. *J. Appl. Phys.* **1991**, *69* (4), 2317–2323.
(14) Chen, G. S.; Boothroyd, C. B.; Humphreys, C. J. *Appl. Phys. Lett.* **1993**, *62*, 1949.
(15) Note that it also can be shrunk by a less focused beam about 100 times lower in current density than the focused one. See also ref 4.
(16) Kimoto, K; Isakozawa, S.; Aoyama, T.; Mataui, Y. *J. Electron Microsc.* **2001**, *50*, 523.
(17) Bullough, T. J.; Devenish, R. W.; Humphreys, C. J. *Inst. Phys. Conf. Ser.* **1990**, *98*, 267.
(18) Tang, B. B; Jones, I. P.; Lai, W. S.; Bacon, D. J. *Philos. Mag.* **2005**, *17*, 1805.
(19) Smeets, R. M. M.; Keyser, U. F.; Wu, M. Y.; Dekker, N. H.; Dekker, C. *Phys. Rev. Lett.* **2006**, *97*, 088101.
(20) Chen, P.; Mitsui, T.; Farmer, D. B.; Golovchenko, J.; Gordon, R. G.; Branton, D. *Nano Lett.* **2004**, *4*, 1333.

NL803613S